ACS APPLIED MATERIALS & INTERFACES

Research Article

www.acsami.org

Band Gap Engineering of Zinc Selenide Thin Films Through Alloying with Cadmium Telluride

M. F. Al-Kuhaili,*[,†] A. Kayani,[‡] S. M. A. Durrani,[†] I. A. Bakhtiari,[†] and M. B. Haider[†]

[†]Physics Department, King Fahd University of Petroleum and Minerals, Dhahran 31261, Saudi Arabia

[‡]Physics Department, Western Michigan University, Kalamazoo, Michigan 49008, United States

ABSTRACT: This work investigates band gap engineering of zinc selenide (ZnSe) thin films. This was achieved by mixing ZnSe with cadmium telluride (CdTe). The mass ratio (x) of CdTe in the starting material was varied in the range x = 0−0.333. The films were prepared using thermal evaporation. The chemical composition of the films was investigated through energy dispersive spectroscopy and Rutherford backscattering spectrometry. Structural analysis was carried out using X-ray diffraction and atomic force microscopy. Normal incidence transmittance and reflectance were measured over the wavelength range 300−1300 nm. The absorption coefficients and band gaps were determined from these spectrophotometric measurements. The band gap monotonically decreased from 2.58 eV (for x = 0) to 1.75 eV (for x = 0.333). Photocurrent measurements indicated that the maximum current density was obtained for films with x = 0.286. A figure of merit, based on crystallinity, band gap, and photocurrent, was defined. The optimum characteristics were obtained for the films with x = 0.231, for which the band gap was 2.14 eV.

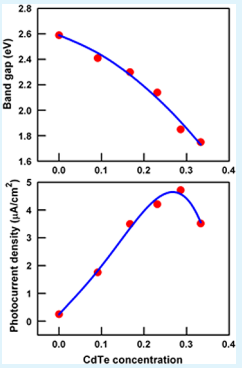

KEYWORDS: *zinc selenide, cadmium telluride, band gap, evaporation, characterization*

1. INTRODUCTION

Zinc selenide (ZnSe) is a compound semiconductor that is characterized by a wide band gap (2.7 eV), high refractive index, low visible absorption, and significant photosensitivity.[1,2] Thus, it has found commercial and potential applications in the fabrication of optoelectronic devices including: (i) blue and infrared laser diodes, (ii) white light emitting diodes (LEDs), (iii) photodetectors, and (iv) as a window layer in heterojunction solar cells.[1−3] All of these applications are critically dependent on the value of the band gap energy of the material. Indeed, numerous applications require band gap values that are not available using binary semiconductor compounds. For example, in solar energy applications, no material system is well tuned for the conversion of photons, with energies in the range 2.3−2.5 eV, into electrons.[4] This energy range is crucial for achieving efficiencies that exceed 50% in multijunction solar cells.[4] In addition, there is still a need for green LEDs with emissions in the energy range 2.21−2.23 eV.[4] Therefore, the ability to tune (or engineer) the band gap is essential for the fabrication of optoelectronic devices with widely varying properties.[5]

Several approaches have been developed to tune the band gap of ZnSe: two approaches are based on recent advances in nanotechnology, whereas the third approach is the traditional technique of composition modulation. The first approach is based on the control of the size and shape of ZnSe nanostructures. When the solid particle size is reduced, or the structure is transformed from a thin film into a spherical dot, the band gap increases.[6] This is called size-induced blue shift.[6] The application of this approach to ZnSe was reviewed in ref 6. The second approach is based on core/shell semiconductor nanostructures, the so-called type II quantum dots.[7] These structures are composed of two semiconductor materials in which the valence and conduction bands in the core are lower (or higher) than those in the shell.[8] This leads to segregation of the electrons and holes between the core and shell materials, which subsequently results in significant tuning of the band gap of the core material.[7] The third approach is composition modulation through doping with impurity atoms, or mixing with other binary semiconductors. Doping results in the substitution of the anions or cations by the impurity atoms, with a corresponding variation in the band gap of the material. Copper[9] and nitrogen[10] were investigated as dopants in ZnSe. However, the resulting change in the band gap of ZnSe was minimal: 0.02 eV for copper and 0.056 eV for nitrogen. A more efficient technique of tuning the band gap over a wide range is the alloying of two binary semiconductors. In this case, engineering the band gap is possible when a solid solution is prepared from two semiconductors with distinct band gaps in their pure form.[11] Isovalent ternary semiconductor alloys $AB_{1-x}C_x$ have been under extensive studies in the last few decades because their physical properties can be tailored for specific applications by changing the alloy composition.[12] However, to have an additional degree of freedom, one can use quaternary alloys $A_xB_{1-x}C_yD_{1-y}$ with adjustable x and y compositions.[13] Ternary alloys of ZnSe and PbSe were synthesized by coevaporation, resulting in a continuous tuning of the band gap from 2.7 down to 1.0 eV.[14] Moreover,

Received: April 18, 2013
Accepted: May 20, 2013
Published: May 20, 2013

   dx.doi.org/10.1021/am4014083 | *ACS Appl. Mater. Interfaces* 2013, 5, 5366−5372

Table 1. Chemical Analysis of the Films

starting materials			atomic concentrations							
			zinc		selenium		cadmium		tellurium	
ZnSe (g)	CdTe (g)	x^a	powder	film	powder	film	powder	film	powder	film
2.0	0	0	0.500	0.460	0.500	0.540	0	0	0	0
2.0	0.2	0.091	0.472	0.410	0.472	0.515	0.028	0.038	0.028	0.037
2.0	0.4	0.167	0.446	0.357	0.446	0.475	0.054	0.085	0.054	0.083
2.0	0.6	0.231	0.424	0.313	0.424	0.449	0.076	0.119	0.076	0.119
2.0	0.8	0.286	0.403	0.242	0.403	0.379	0.097	0.190	0.097	0.188
2.0	1.0	0.333	0.384	0.189	0.384	0.317	0.116	0.240	0.116	0.254
0	2.0	1	0	0	0	0	0.500	0.496	0.500	0.504

[a]Ratio of the mass of CdTe to the total mass of the powder.

quaternary ZnCdSeTe nanowires with tunable band gaps were grown by molecular beam epitaxy for photodetector applications.[15]

In this work, band gap engineering of ZnSe thin films was achieved by mixing it with cadmium telluride (CdTe). This material, with a band gap of 1.5 eV, has received tremendous interest in photovoltaics because its band gap is close to the optimum value for the maximum efficiency of light-to-electricity conversion.[16] Both ZnSe and CdTe are II−VI semiconductors with cubic zincblende crystal structure and direct band gaps, which offer high oscillator strengths for optical transitions.[17] The films in this work were deposited using thermal evaporation of ZnSe powders mixed with specific concentrations of CdTe.

2. EXPERIMENTAL DETAILS

The starting materials were powders of ZnSe and CdTe (Balzers, 99.99% purity). In all depositions, the mass of the ZnSe powder was 2.0 g. Various concentrations of CdTe were added to the ZnSe powder with corresponding ratios as shown in Table 1. The powders were homogeneously mixed in a sonicator. Throughout the paper, the ratio of the mass of CdTe to the total mass of the mixed powder will be represented by x, and results will be presented in terms of this quantity since it is the experimentally measured and controlled quantity. The films were prepared in a Leybold L560 box coater and were deposited on unheated fused silica substrates, by thermal evaporation of the powders from a molybdenum boat. The film thickness and rate of evaporation were controlled using a quartz crystal thickness monitor. The rate of evaporation was 0.2 nm/s, and the films thickness was 175 ± 6 nm, as measured by a stylus surface profilometer (Ambios XP2).

The chemical composition of the films was determined using energy dispersive spectroscopy (EDS) and Rutherford backscattering spectrometry (RBS). EDS was performed in a JEOL 5800 LV scanning electron microscope. RBS measurements were performed using a 2.5 MeV beam of He^{2+} ions. The incidence angle measured from the sample normal was 0°. Backscattered ions were collected using a silicon surface barrier detector at a scattering angle of 150°, with an exit angle of 30°. The structural properties of the films were investigated using X-ray diffraction (XRD), which was carried out in a Rigaku Ultima IV diffractometer employing Cu Kα radiation. The 2θ step and step acquisition time were 0.02° and 1.00 s, respectively. The surface morphology of the films was examined using contact mode atomic force microscopy (AFM, Veeco Innova diSPM). The sample surface was probed with a silicon tip of 10 nm radius oscillating at its resonant frequency of 300 kHz. The scan area was 0.5 μm × 0.5 μm, and the scan rate was 2 Hz. Normal-incidence transmittance and reflectance of the films were measured over the wavelength range 300−1300 nm using a Jasco V570 double-beam spectrophotometer. Photocurrent measurements were carried out at room temperature in a dark chamber. Light from a xenon arc lamp was dispersed by a monochromator (AMINCO SPF-500) to get the excitation wavelength of 480 nm. For current measurements, two gold electrodes, with a spacing of 1 mm, were deposited on the surfaces of the films, and the current was measured, under a bias voltage of 20 V, using a Keithley 238 source measure unit.

3. RESULTS AND DISCUSSION

Chemical Analysis. The elemental composition of the films was determined by EDS and was carried out only for Zn, Se, Cd, and Te. The results of chemical analysis are shown in Table 1. For comparison, the atomic concentrations of the elements in the mixed films are shown in Figure 1. For pure ZnSe thin films, the atomic concentration of Zn was lower than that of Te. This may be explained by considering the vapor pressures of the two elements, as shown in Figure 2a. For thermally evaporated II−VI semiconductors, the compounds decompose into their constituent elements during evaporation.[21] Since the vapor pressure of Se is higher, the atomic concentration of Zn will be lower. Moreover, the sticking coefficient of Zn is lower than that of Se.[22] On the other hand, pure CdTe thin films preserve the stoichiometric ratio of the elements in the film, despite the larger vapor pressure of Cd. This may be attributed to the observation that the sticking coefficients of Cd and Te approach 100%, and that it is only through the formation of CdTe that these elements exist on the substrate surface.[23]

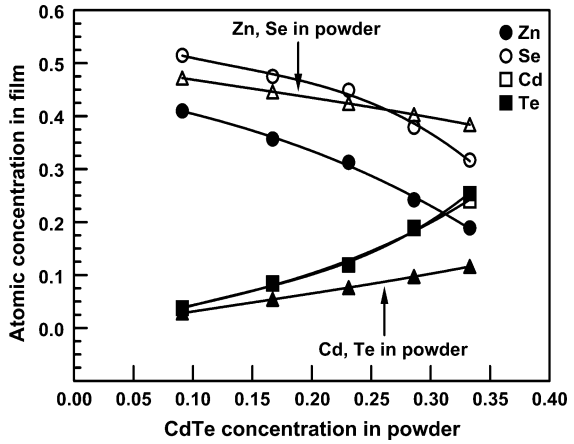

Figure 1. Atomic concentrations of the elements in the alloyed films as determined by EDS.

Several observations can be made regarding the chemical composition of the mixed films. First, the atomic concentration of Zn was significantly lower than its value in the starting powder, indicating a lack of Zn incorporation. This problem has been observed in Zn-based II−VI alloyed films and was attributed to the low sticking coefficient of Zn.[24] It was

dx.doi.org/10.1021/am4014083 | ACS Appl. Mater. Interfaces 2013, 5, 5366−5372

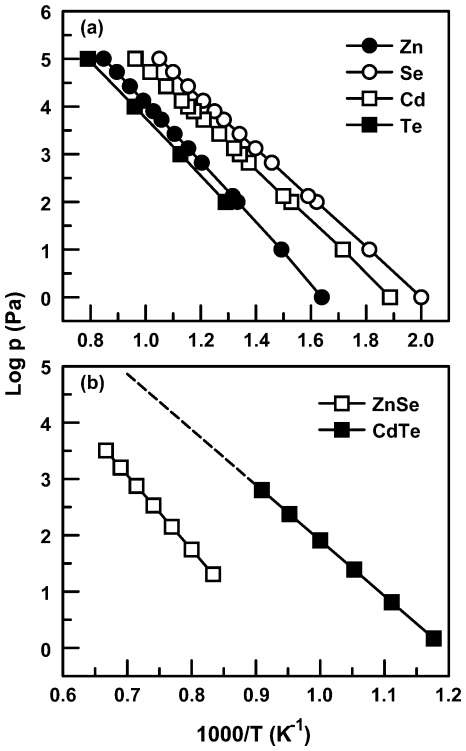

Figure 2. (a) Vapor pressures of the elements Cd, Se, Te, and Zn. Values are taken from refs 18 and 19. (b) Vapor pressures of CdTe and ZnSe. Values are taken from ref 20.

observed that Zn sticks only to Se atoms,[25] and thus with increasing Cd and Te concentrations, the sticking probability of Zn was lowered. Second, Cd and Te preserved their stoichiometric ratio (1:1) in the mixed films. Third, the atomic concentrations of Cd and Te in the films were significantly higher than their values in the starting powder. This may be attributed to the higher vapor pressure of CdTe, compared to ZnSe (see Figure 2b). This also explains the decrease in the atomic concentration of Se. Fourth, the rate of increase of the atomic concentrations of Cd and Te in the alloyed films was not linear (as in the powder), but rather followed a steeper trend. This can be explained by considering the dynamics of the evaporation process. In our experiments, the final thickness and deposition rate were set by the quartz crystal thickness monitor. Thus, the evaporation time was fixed. The vapor pressure of CdTe is higher. As a result, when ZnSe starts evaporating, CdTe has already started evaporation, and consequently, the rate of evaporation of CdTe is higher and it depletes faster. For the lowest concentrations of CdTe in the powder, it will deplete before the final thickness is achieved. For higher concentrations of CdTe in the powder, it will be present until the end of evaporation. Since its rate of evaporation is higher, the atomic concentrations of its constituents in the film are higher than those in the powder, and their rate of increase is steeper. These observations are further supported by RBS.

Figure 3 shows typical RBS overlaid spectra of five different samples, including pure ZnSe, mixed films with x = 0.091, 0.231, 0.333, and pure CdTe. The first (lower-energy) peak contains the concentration information for Zn and Se, with the leading edge representing Se (being the heavier of the two elements). The second (higher-energy) peak provides the elemental concentration of Cd and Te, with the leading edge representing Te. RBS is particularly useful in determining the

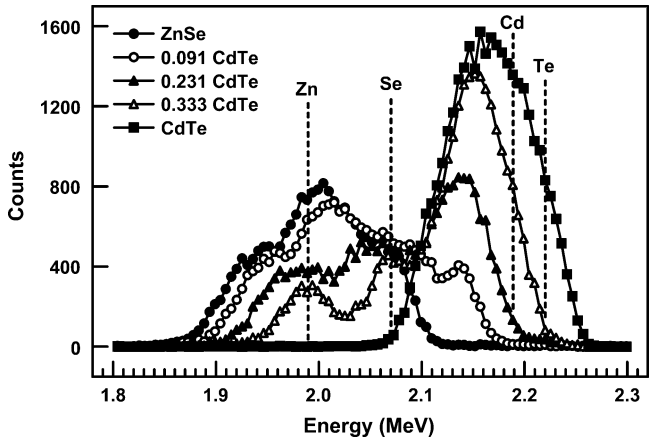

Figure 3. Typical RBS spectra of the films.

depth profile of a known element, and whether it exits on the surface or buried deeper in the film. In the case of a buried element, the resulting peak shifts toward lower energy with respect to the surface energy position. The spectra in Figure 3 show peak edges representing Zn and Se at the representative surface energy of the two elements and the leading edge (Se edge) remains fixed in the spectra of all the samples. However, the edge of the peak representing Cd and Te presents an interesting trend. As the percentage of CdTe in ZnSe is increased, the leading edge of the peak (Te edge) moves toward higher energy and reaches the surface energy of Te in the pure CdTe sample. This indicates that both Cd and Te are buried in the film and gradually move toward the surface. This corroborates our assumption on the evaporation dynamics presented above.

Structural Analysis. The XRD patterns of the films are shown in Figure 4, and they exhibit the polycrystalline nature of the films. The XRD pattern of the pure ZnSe thin films shows a predominant peak at 2θ = 27.17°, which is in accordance with the standard XRD data on ZnSe powder.[26] This peak indicates that the crystallites are preferentially oriented along the (111)

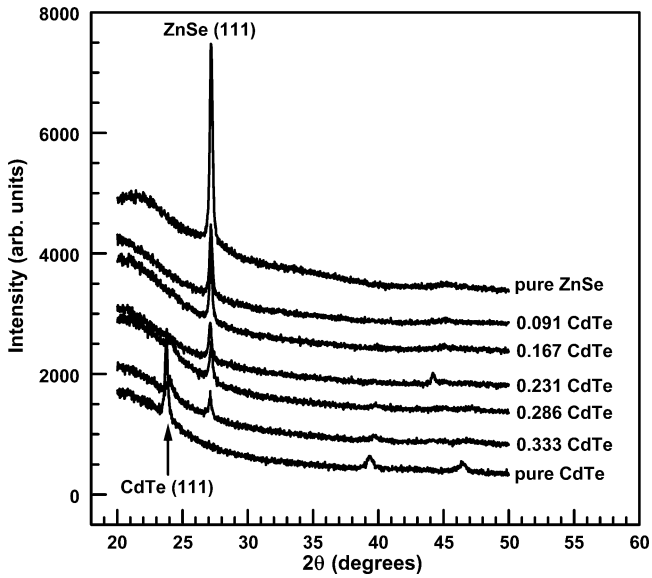

Figure 4. XRD patterns of the films. The numbers on the spectra represent the concentration (by mass) of CdTe in the starting material.

dx.doi.org/10.1021/am4014083 | ACS Appl. Mater. Interfaces 2013, 5, 5366−5372

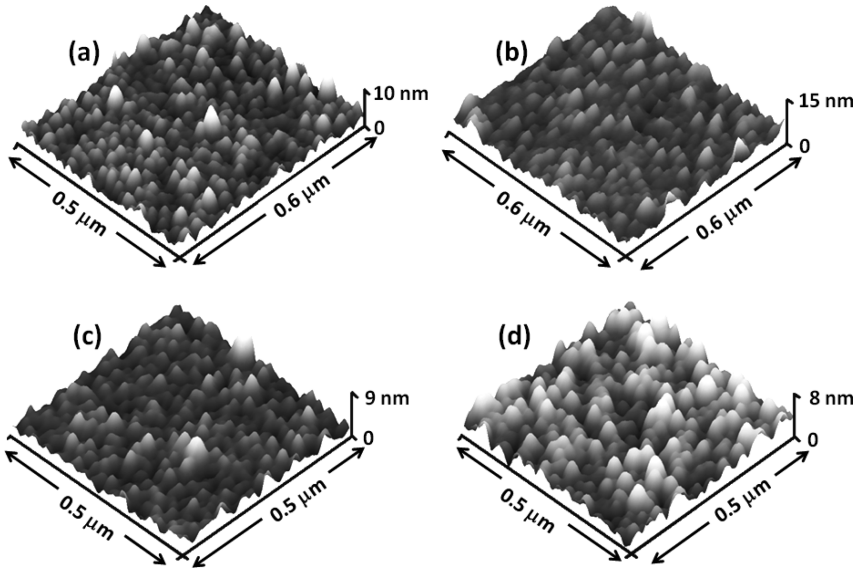

Figure 5. Three dimensional images of the films: (a) pure ZnSe, (b) 0.167 CdTe, (c) 0.333 CdTe, (d) pure CdTe.

direction, which is the close packing direction of the cubic zinc blende structure.[27] The crystallite size was estimated from the Scherrer formula, and was found to be 35.1 nm. Similarly, the XRD pattern of the pure CdTe thin films shows a predominant peak at $2\theta = 23.73°$, corresponding to the (111) direction of CdTe,[26] with a crystallite size of 36.4 nm.

Addition of CdTe into ZnSe resulted in deterioration of crystallinity, as evidenced by the decrease in XRD peak intensity, and the reduction in crystallite size to a value of 22.7 nm for the films with the highest CdTe concentration. For films with $x \leq 0.286$, there were no XRD peaks corresponding to CdTe. However, the films with the highest CdTe concentration (0.333) indicated the presence of both ZnSe and CdTe in crystalline form and, thus, phase separation. In our films, the degree of crystallinity was limited by (i) the low kinetic energies of the evaporated species, (ii) the low thickness of the films, and (iii) the deposition on unheated amorphous substrates. The degradation of crystallinity with increased mixing may be explained by the segregation of CdTe into the grain boundaries of ZnSe, and its tendency to create nucleation centers.[28,29] Another factor is the lack of incorporation of Zn, and the corresponding excess of Se. The lack of XRD peaks belonging to CdTe in samples with $x \leq 0.286$ may be attributed to the small density of CdTe crystallites in these samples, which may be lower than the XRD detection limits.

Atomic force microscopy images of the films are shown in Figure 5. The surface morphology of the films showed columnar structure, which is similar to previous reports on evaporated ZnSe and CdTe thin films.[30,31] Statistical analysis of the images was performed to obtain the root-mean-square roughness of the films, which was found to be 1.2 ± 0.2 nm indicating the growth of films with smooth surfaces. This roughness is similar to the value of 1.522 nm reported for thermally evaporated ZnSe thin films.[10]

Band Gap. The transmittance (T) and reflectance (R) spectra of the films are shown in Figures 6 and 7, respectively. The absorption edges of the films were red-shifted as the concentration of CdTe increased. The films were transparent in the near-infrared region. The absorption coefficient (α) can be obtained from these spectra using the relation:

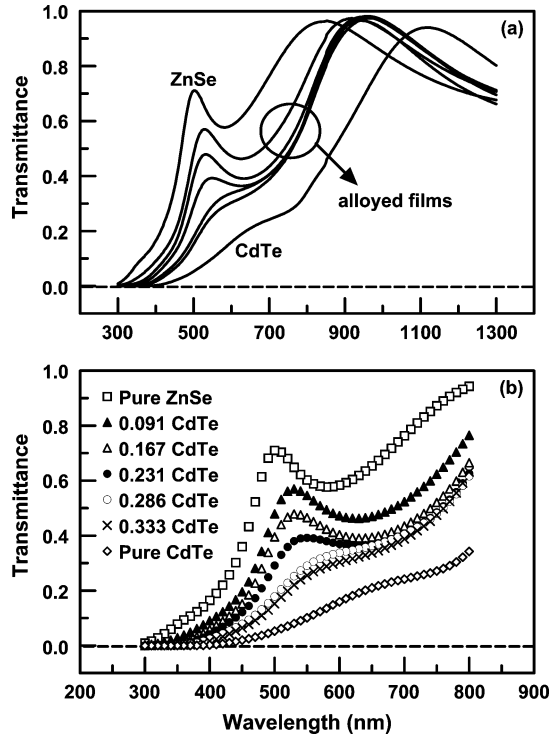

Figure 6. (a) Transmittance spectra of the films over the full wavelength measurement range. (b) Enlarged view of the transmittance spectra over the visible range. The numbers on the curves represent the concentration (by mass) of CdTe in the starting material.

$$T = \frac{(1 - R)\exp(-\alpha d)}{1 - [R^2\exp(-2\alpha d)]} \quad (1)$$

In the fundamental absorption region, the second term in the denominator of eq 1 is negligible. Therefore, eq 1 can be rewritten as $T \approx (1 - R)e^{-\alpha d}$. From which,

$$\alpha = \frac{1}{d}\ln\left(\frac{1 - R}{T}\right) \quad (2)$$

dx.doi.org/10.1021/am4014083 | ACS Appl. Mater. Interfaces 2013, 5, 5366−5372

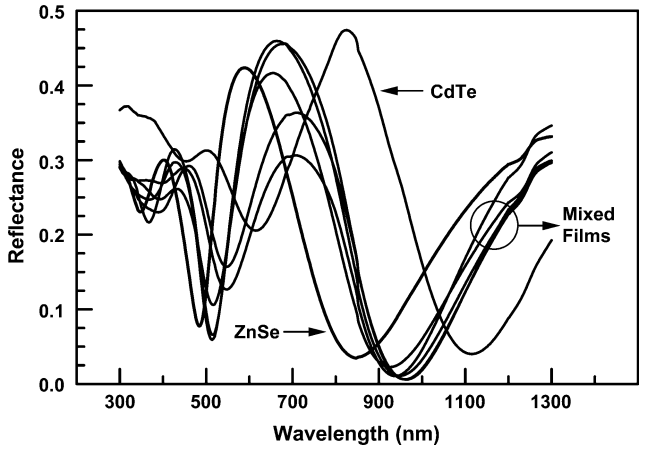

Figure 7. Reflectance spectra of the films.

The absorption coefficient was calculated using eq 2, and the results are shown in Figure 8.

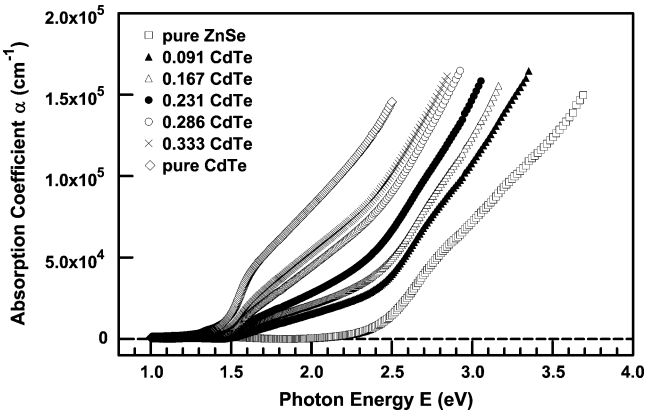

Figure 8. Absorption coefficients of the films. The numbers on the curves represent the concentration (by mass) of CdTe in the starting material.

The absorption coefficient is related to the band gap (E_g) by the relation:

$$\alpha = \frac{\alpha_o}{E}(E - E_g)^{\eta} \quad (3)$$

where α_o is a constant and E is the incident photon energy. The constant η depends on the type of transitions involved, and its value is $\eta = 1/2$ for direct allowed transitions. In order to obtain the band gap, $(\alpha E)^2$ is plotted as a function of photon energy. The linear portions of the curves are fitted using linear regression analysis. An extrapolation of the linear regions of the plots gives the value of the band gap as the intercept to the horizontal axis (where $\alpha E = 0$). Such plots are shown in Figure 9. The band gap of pure ZnSe thin films was found to be 2.59 eV, which is close to the values of 2.6−2.7 eV reported for evaporated ZnSe thin films.[27,28] The band gap of pure CdTe thin films was found to be 1.53 eV, in agreement with the value of 1.534 eV reported for evaporated CdTe thin films.[32] The band gap of the mixed films decreased as the concentration of CdTe increased, as shown in Figure 10. The variation of the band gap with CdTe concentration may be fitted using a relation of the form:[33]

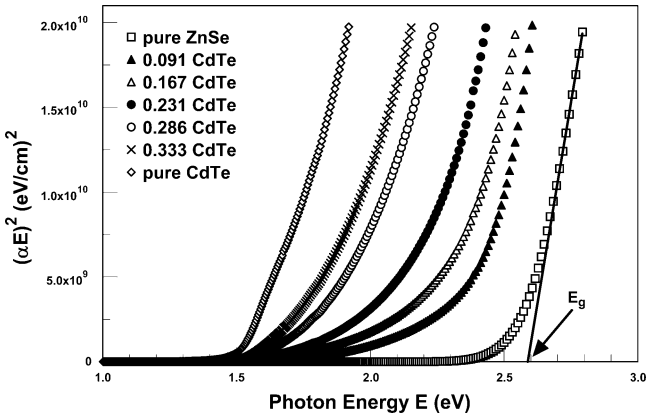

Figure 9. Plots of $(\alpha E)^2$ versus photon energy for band gap determination. The numbers on the curves represent the concentration (by mass) of CdTe in the starting material.

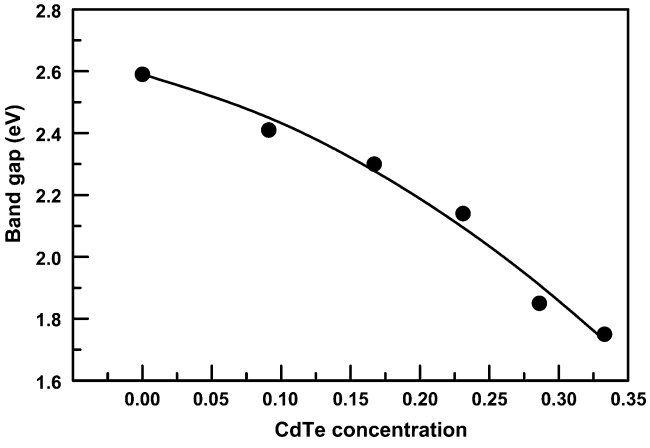

Figure 10. Variation of the band gap with CdTe concentration.

$$E_g(x) = E_g(0) + ax + bx^2 \quad (4)$$

where $E_g(0)$ is the band gap of ZnSe thin films, and a and b are constants. Least-squares fitting of this relation to our data is shown by the continuous curve in Figure 10, where the best-fit parameters were found to be $a = 1.15$ eV and $b = -4.29$ eV.

Photocurrent. Figure 11 shows the photocurrent density (J_{pc}) of the films as a function of the CdTe concentration. The

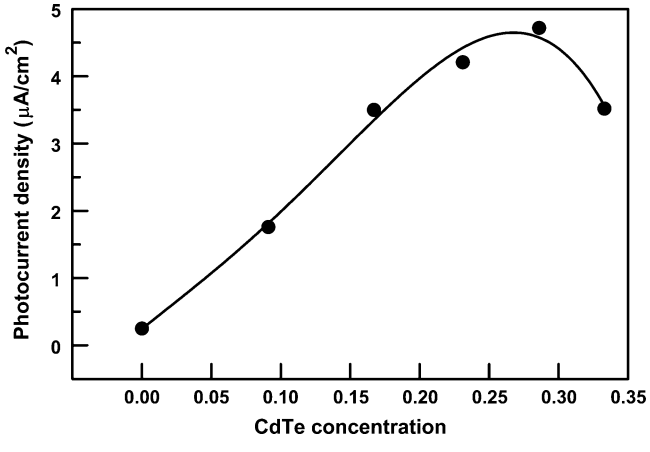

Figure 11. Photocurrent density of the films as a function of the mass concentration of CdTe in the starting powder.

dx.doi.org/10.1021/am4014083 | ACS Appl. Mater. Interfaces 2013, 5, 5366−5372

photocurrent density increased steadily up to x = 0.286 but then decreased for the highest CdTe concentration. Absorption of photons under an applied electric field results in the generation of electron−hole pairs that constitute the photocurrent. J_{pc} increased as the band gap decreased, which can be understood by the fact that photons, of a given energy that is higher than the band gap, can generate more electron−hole pairs as the band gap is decreased due to the increased density of states in both the conduction and valence bands. This trend did not seem to be affected by the crystallinity of the films. The decrease of J_{pc} for the highest CdTe concentration may be attributed to the presence of two different crystalline phases in these films, which leads to the trapping of photogenerated charge carriers, and increases the scattering of these carriers at grain boundaries.[34,35]

Discussion. Our results showed that there was a continuous and tunable reduction of the band gap as the cadmium telluride concentration increased. This is very desirable for solar energy applications. However, there are other important factors such as crystallinity and photocurrent. A decision on the suitability of the films for device applications must take all these factors into consideration. Thus, we may define a figure of merit (Φ), based on these factors, as follows:

$$\Phi = \frac{LJ_{pc}}{E_g} \tag{5}$$

where L is the crystallite size. The figure of merit is plotted as a function of the concentration of cadmium telluride in Figure 12. It clearly shows that the optimum value was obtained in the films with a CdTe concentration of 0.231.

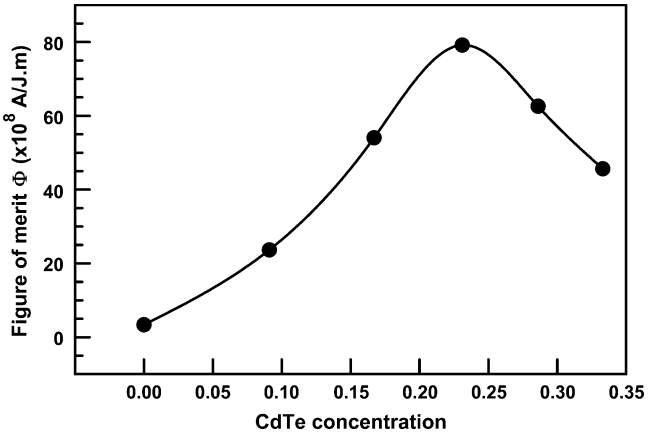

Figure 12. Figure of merit as a function of CdTe concentration.

4. CONCLUSION

Band gap engineering of ZnSe was achieved by mixing it with CdTe. The mass concentration (x) of CdTe in the starting material was varied from 0 to 0.333. The atomic concentrations of the elements in the films were different from their values in the starting material. Moreover, the elements were not uniformly distributed throughout the films. Pure ZnSe and CdTe thin films were polycrystalline. The crystallinity was deteriorated as the concentration of CdTe increased. However, for the highest CdTe concentration, both ZnSe and CdTe crystalline phases coexisted. The films possessed columnar structure with smooth surfaces. The absorption edges of the films were red-shifted with the increase in CdTe concentration. Band gap values showed a continuous quadratic variation with the increases in CdTe concentration. The band gap values decreased from 2.58 eV for pure ZnSe thin films to 1.75 eV for the films with x = 0.333. Photocurrent density had a maximum value for the films with x = 0.286. It was mainly affected by the band gap. Finally, a figure of merit based on crystallinity, band gap and photocurrent was defined, from which the films with x = 0.231 showed optimum characteristics.

AUTHOR INFORMATION

Corresponding Author

*Tel.: 96638602278. Fax: 96638602293. E-mail: kuhaili@kfupm.edu.sa.

Notes

The authors declare no competing financial interest.

ACKNOWLEDGMENTS

The support to this work by the Physics Department and the Research Institute of King Fahd University of Petroleum and Minerals is acknowledged.

REFERENCES

(1) Sadekar, H. K.; Ghule, A. V.; Sharma, R. *Compos. Pt. B-Eng.* **2013**, *44*, 553−557.
(2) Evans, J. W.; Berry, P. A.; Schepler, K. L. *Opt. Lett.* **2012**, *37*, 5021−5023.
(3) Rao, K. G.; Bangera, K. V.; Shivakumar, G. K. *Solid State Sci.* **2011**, *13*, 1921−1925.
(4) Agarwal, S.; Montgomery, K. H.; Boykin, T. B.; Klimeck, G.; Woodall, J. M. *Electrochem. Solid State Lett.* **2010**, *13*, H5−H7.
(5) Little, M. E.; Kordesch, M. E. *Appl. Phys. Lett.* **2001**, *78*, 2891−2892.
(6) Chen, Y.; Li, J.; Yang, X.; Zhou, Z.; Sun, C. Q. *J. Phys. Chem. C* **2011**, *115*, 23338−23343.
(7) Smith, A. M.; Nie, S. *Acc. Chem. Res.* **2010**, *43*, 190−200.
(8) Bang, J.; Park, J.; Lee, J.; Won, N. W.; Nam, J.; Lim, J.; Bang, B.; Lee, H.; Chon, B.; Shin, J.; Park, J.; Choi, J.; Cho, K.; Park, S.; Joo, T.; Kim, S. *Chem. Mater.* **2010**, *22*, 233−240.
(9) Ali, Z.; Aqili, A. K.; Maqsood, A.; Akhtar, S. M. *Vacuum* **2005**, *80*, 302−309.
(10) Venkatachalam, S.; Mangalaraj, D.; Narayandass, S. K.; Kesavamoorthy, R.; Magudapathy, P.; Sundaravel, B.; Kalavathi, S.; Nair, K. G. *Semicond. Sci. Technol.* **2006**, *21*, 1661−1667.
(11) Lehr, D.; Luka, M.; Wagner, M. R.; Bugler, M.; Hoffmann, A.; Polarz, S. *Chem. Mater.* **2012**, *24*, 1771−1778.
(12) Moon, C. Y.; Wei, S. H.; Zhu, Y. Z.; G. D. Chen, G. D. *Phys. Rev. B* **2006**, *74*, 233202.
(13) Mezrag, F.; Bouarissa, N.; Boucenna, M.; Hannachi, L. *Phys. Script.* **2010**, *82*, 035702.
(14) Abe, S. *Nanoscale Res. Lett.* **2011**, *6*, 324−329.
(15) Chang, S. J.; Hsiao, C. H.; Wang, S. B.; Cheng, Y. C.; Li, T. C.; Chang, S. P.; Huang, B. R.; Hung, S. C. *Nanoscale Res. Lett.* **2009**, *4*, 1540−1546.
(16) Miles, R.; Hynes, K.; Forbes, I. *Prog. Cryst. Growth Charact. Mater.* **2005**, *51*, 1−42.
(17) Ladd, T. D.; Sanaka, K.; Yamamoto, Y.; Pawlis, A.; Lischka, K. *Phys. Status Solidi B* **2010**, *247*, 1543−1546.
(18) Cohen, E. R., Lide, D. R., Trigg, G. L., Ed. *AIP Physics Desk Reference*, 3rd ed.; Springer-Verlag: New York, 2003.
(19) Green, D. W., Ed. *Perry's Chemical Engineers' Handbook*, 8th ed.; McGraw-Hill: New York, 2008.
(20) Predel, B., Ed. *Springer Materials - The Landolt-Börnstein Database*; Springer-Verlag: Berlin Heidelberg, 2012; http://www.springermaterials.com.
(21) Ritter, E. *Appl. Opt.* **1976**, *15*, 2318−2327.

(22) Okuyama, H.; Kijima, S.; Sanaka, Y.; Ishibashi, A. *J. Cryst. Growth* **1998**, *193*, 43−49.
(23) Neretina, S.; Hughes, R. A.; Britten, J. F.; Sochinskii, N. V.; Preston, J. S.; Mascher, P. *Nanotechnology* **2007**, *18*, 275301.
(24) Dhere, R.; Gessert, T.; Zhou, J.; Asher, S.; Pankow, J.; Moutinho, H. *Investigation of CdZnTe for Thin-Film Tandem Solar Cell Applications*; National Renewable Energy Laboratory (NREL): Golden, CO, 2003; preprint no. NREL/CP-520-33965.
(25) Yao, T.; Maekawa, S. *J. Cryst. Growth* **1981**, *53*, 423−431.
(26) International Center for Diffraction Data (ICDD): file no. 00-001-090 for ZnSe and file no. 00-010-0207 for CdTe.
(27) Venkatachalam, S.; Mangalaraj, D.; Narayandass, S. K.; Kim, K.; Yi, J. *Phys. B* **2005**, *358*, 27−35.
(28) Lee, J. H.; Park, B. O. *Thin Solid Films* **2003**, *426*, 94−99.
(29) Tahar, R. B. *J. Eur. Ceram. Soc.* **2005**, *25*, 3301−3306.
(30) Rusu, G. I.; Diciu, M.; Pirghie, C.; Popa, E. M. *Appl. Surf. Sci.* **2007**, *253*, 9500−9505.
(31) Luschitz, J.; Siepchen, B.; Schaffner, J.; Lakus-Wollny, K.; Haindl, G.; Klein, A.; Jaegermann, W. *Thin Solid Films* **2009**, *517*, 2125−2131.
(32) Lalitha, S.; Karazhanov, S. Z.; Ravindran, P.; Senthilarasu, S.; Sathyamoorthy, R.; Janabergenov, J. *Phys. B* **2007**, *387*, 227−238.
(33) Liang, Y.; Zhai, L.; Zhao, X.; Xu, D. *J. Phys. Chem. B* **2005**, *109*, 7120−7123.
(34) Yuliarto, B.; Zhou, H.; Yamada, T.; Honma, I.; Katsumura, Y.; Ichihara, M. *Anal. Chem.* **2004**, *76*, 6719−6726.
(35) Mridha, S.; Basak, D. *J. Phys. D: Appl. Phys.* **2007**, *40*, 6902−6907.